Supporting Information for:

"Environmental Process Optimisation of an Adsorption-Based Direct Air Carbon Capture and Storage System"

P. Postweiler[a], **M. Engelpracht**[a], **D. Rezo**[a], **A. Gibelhaus**[a], **and N. von der Assen**[a*]

[a]Institute of Technical Thermodynamics, RWTH Aachen University, 52062 Aachen, Germany

[*]Corresponding author: niklas.vonderassen@ltt.rwth-aachen.de

Contents

1. Details of the Investigated Adsorption Cycles

The following describes the <u>T</u>emperature <u>V</u>acuum <u>S</u>wing <u>A</u>dsorption cycle (TVSA) and the <u>S</u>team-assisted <u>T</u>emperature <u>V</u>acuum <u>S</u>wing <u>A</u>dsorption cycle (S-TVSA) in detail. Fig 1 shows the five phases and process design variables of both cycles.

I. **Adsorption phase (ads):** During the adsorption phase with phase duration τ_{ads}, a fan blows an airflow $\dot{m}_{ads}$ through the adsorption column. The airflow has ambient conditions (i.e., temperature T_{amb}, pressure p_{amb}, and relative humidity φ_{amb}). The fan overcomes the pressure drop of the adsorption column and requires the mechanical work $\dot{W}_{fan}$. The selected adsorbent, amine-functionalised cellulose (APDES-NFC), adsorbs CO_2 and H_2O from the airflow at a total pressure near ambient pressure. The heat of adsorption is released to the ambient as the heat flow rate $\dot{Q}_{ads}$ at ambient temperature via the heating and cooling jacket. Thus, an airflow with less CO_2 and H_2O leaves the adsorption column.

II. **Blowdown phase (blow):** The blowdown phase has the phase duration τ_{blow} and starts with closing the inlet of the adsorption column. Then, a vacuum pump decreases the column pressure to the desorption pressure p_{des}, thereby extracting most of the air from the adsorption column. The vacuum pump needs the mechanical work $\dot{W}_{vac,blow}$. The extracted air is released into the environment.

III. **Heating phase (heat):** During the heating phase with phase duration τ_{heat}, the adsorption column is heated by the heat flow rate $\dot{Q}_{heat}$ provided via the heating and cooling jacket. The heat flow rate is mainly used for sensible heating. Due to limited heat transport, the adsorbent slowly heats to the desorption temperature T_{des}. Thereby, mainly H_2O is desorbed due to faster kinetics and beneficial equilibrium loading compared to CO_2. The column pressure is kept constant at the desorption pressure p_{des} via a vacuum pump. The vacuum pump needs the mechanical work $\dot{W}_{vac,heat}$. The phase duration can vary, and for the TVSA there are no restrictions on the minimum duration of the phase.. However, for the S-TVSA, the phase duration must be long enough to heat the adsorbent above the boiling point temperature of water at desorption pressure to prevent condensation on the adsorbent.

IV. **Desorption phase (des), variant 1, TVSA cycle:** During the desorption phase with phase duration τ_{des}, the adsorption column is further heated and maintained constant at the desorption temperature T_{des}. The required heat flow rate $\dot{Q}_{des}$ is mainly used to provide the heat of adsorption. In this phase, mainly CO_2 is desorbed since most H_2O was already desorbed during the heating phase. The mass flow rate $\dot{m}_{des}$ leaves the adsorption column. The remaining water is condensed from the mass flow rate $\dot{m}_{des}$ by cooling it to the ambient temperature T_{amb}. Thereby, the heat flow rate $\dot{Q}_{cond}$ is released to the ambient. Thus, a CO_2-rich product stream leaves the column.

IV. **Desorption phase (des), variant 2, S-TVSA cycle:** During the desorption phase with phase duration τ_{des}, water is heated, evaporated, and superheated by a heat flow rate $\dot{Q}_{evp}$ to the desorption temperature T_{des}. The steam mass flow rate $\dot{m}_{ste}$ enters the adsorption column and has two main effects: i) The adsorbent is heated almost instantaneously due to excellent heat transfer, and ii) desorbed CO_2 is directly displaced by H_2O, which lowers the partial pressure of the CO_2 and thus enhances desorption. The steam is condensed by cooling the mass flow rate $\dot{m}_{des}$ to the ambient temperature T_{amb}. Thereby, the heat flow

rate $\dot{Q}_{cond}$ is released to the ambient, and a CO₂-rich product flow leaves the adsorption column at ambient temperature T_{amb} and pressure p_{amb}.
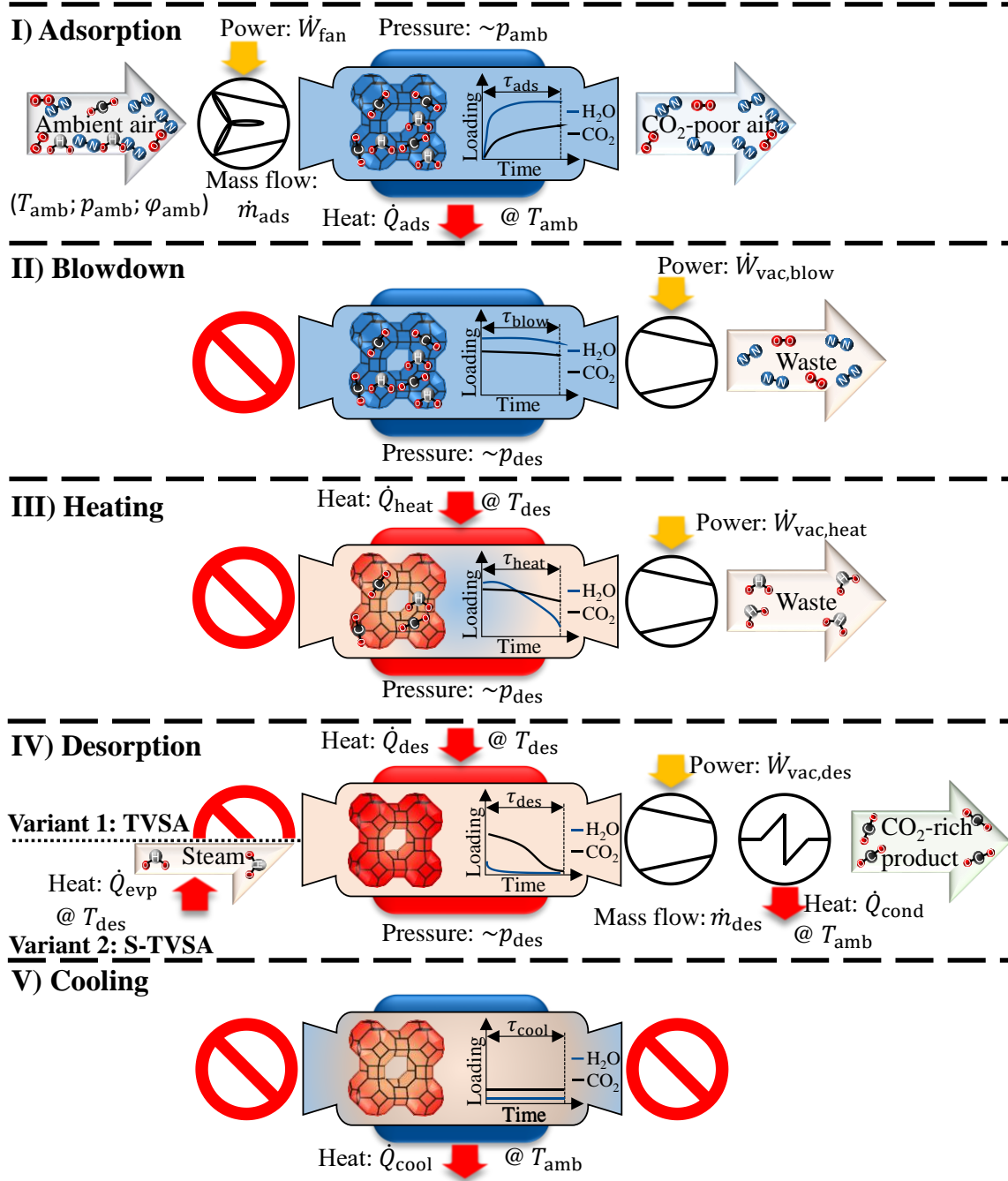
Fig 1 The five phases of a Temperature Vacuum Swing Adsorption cycle (TVSA) and a Steam-assisted Temperature Vacuum Swing Adsorption cycle (S-TVSA) for DAC were adapted from Young et al.[1]. I) Adsorption: A fan blows ambient air through the adsorption column; CO₂ and H₂O are adsorbed. II) Blowdown: A vacuum pump decreases the column pressure to desorption pressure as the column inlet is closed. III) Heating: A jacket heats the column to the desorption temperature. IV) Desorption via the TVSA cycle: Extraction of CO₂ with closed column inlet; or desorption via the S-TVSA cycle: Extraction of CO₂ by injecting superheated steam. V) Cooling: Cooling of the adsorption column before the next adsorption phase to avoid sorbent degradation.

IV. **Cooling phase (cool):**

From a process point of view, there is no need for a cooling phase as the incoming airflow rapidly cools the adsorption column to ambient temperature. However, amine-functionalised materials tend to degrade at high temperatures and high oxygen concentrations oxidatively.[2,3] Thus, Young et al. proposed extending the four-phase TVSA cycle by a fifth phase, the cooling phase, to extend the lifetime of the adsorbent.[1] Here, the heat flow rate $\dot{Q}_{cool}$ cools the adsorption column with its inlet and outlet valves closed. Once the average adsorbent temperature $\bar{T}_{sor}$ is below 90 °C, the cooling phase ends.

Overall, the ambient conditions (i.e., temperature T_{amb}, pressure p_{amb}, and relative humidity φ_{amb}) defined the investigated case study and were fixed. The process control (i.e., mass flow $\dot{m}_{ads}$; phase times τ_{ads}, τ_{blow}, τ_{heat}, and τ_{des}; and desorption conditions p_{des}, T_{des}, $\dot{m}_{ste}$) were degrees of freedom of the process design.

2. Details of the Dynamic Model

Fig. 2 shows a scheme of an adsorption column (top) and the corresponding structure of our dynamic model (bottom). The adsorption column was filled with a porous adsorbent, with the void filled by a gas phase. The model's adsorbent and gas volumes were represented in the same spatial cell. The two volumes (i.e., gas volume and adsorbent cell) interacted via mass and heat transfers.
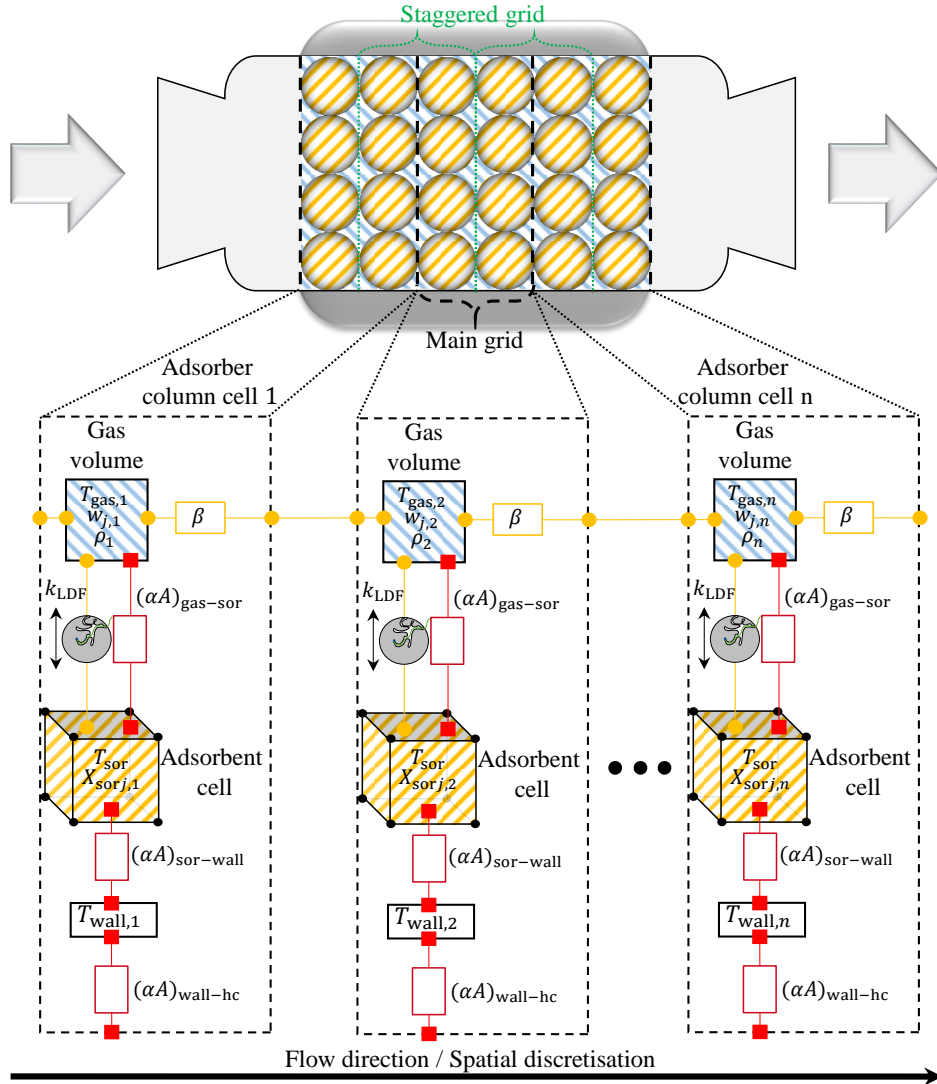
Fig. 2 **Scheme of the adsorption column and its dynamic model. The gas volume is shaded blue, and the adsorbent cell is shaded orange. The 1D staggered grid upwind type finite volume discretisation is illustrated by three cells.**

Fig. 2 also provides insights into the spatial discretisation of the model. The adsorption column was 1D discretised in the flow direction. We used an upwind type finite volume method combined with a staggered grid approach[4] as the discretisation method to keep the model numerically efficient and robust. In a standard upwind type finite volume approach, the grid defines a finite volume, and all quantities are calculated as average values in this volume (e.g., temperature T or mass fraction w_j). These average values are passed to the next cell in the flow direction. In contrast, the staggered grid approach places a second grid over the same space, allowing to split some calculations: The momentum balance is calculated on the additional grid. Thus, the convective mass transport represents a separate spatial cell going from the center of the ith spatial cell to the center of the $i^{th} + 1$ cell. Shifting the momentum balance to the staggered grid reduces the index of the Differential-Algebraic system of Equations (DAE) and, thus, the DAE is solved more efficiently and robustly by the solver.[5]

The dynamic adsorption column model was based on the following main assumptions:

- Radial temperature and concentration gradients are negligible, allowing for a 1D discretisation in the flow direction.
- Axial dispersion due to concentration gradients is negligible.

5

- Axial thermal conductivity is negligible.
- All heat transfer coefficients are constant.
- The gas phase is an ideal gas/mixture.
- The mass transport between the gas phase and the adsorbent depends neither on the temperature, the gas mixture, nor the loading, and a first-order linear driving force approach is sufficient for the CO_2 and H_2O adsorption kinetics.

In order to provide more insight into the dynamic adsorption column model, Tab. 1 summarises all equations of the differential-algebraic system of equations. The notation $\begin{cases} Z_{x,i-1}, & \dot{m}_x \geq 0 \\ Z_{x,i}, & \dot{m}_x < 0 \end{cases}$ in the balance equations refers to the used upwind discretisation scheme. According to the upwind discretisation scheme, a mass flow rate entering the cell i coming from the cell $i-1$ ($\dot{m}_x \geq 0$) holds the state quantities of the previous cell $Z_{x,i-1}$ while a mass flow leaving the cell i in the direction of cell $i-1$ ($\dot{m}_x < 0$) has the state quantities $Z_{x,i}$ of the current cell i.

Tab. 1   Full set of the differential-algebraic system of equations used for the dynamic adsorption column model. The variable naming and indices are based on Fig. 2.

Model for the mass transfer

From gas volume i to adsorbent cell i (LDF approach)	$\dot{m}_{\text{LDF},i,j} = m_{\text{sor},i} k_{\text{LDF},i,j}\left[X_{i,j}(p,T,y_i) - X_{\text{sor},i,j}\right]$	(S1)

From gas volume i to gas volume $i+1$ (convective flow)	$\dot{m}_{\text{conv},i} = f([p_{i+1} - p_i])$	(S2)

Model for the heat transfer

From gas volume i to adsorbent cell i	$\dot{Q}_{\text{gas}-\text{sor},i} = (\alpha A)_{\text{gas}-\text{sor},i}\left[T_{\text{gas},i} - T_{\text{sor},i}\right]$	(S3)

From adsorbent cell i to wall cell i	$\dot{Q}_{\text{sor}-\text{wall},i} = (\alpha A)_{\text{sor}-\text{wall},i}\left[T_{\text{sor},i} - T_{\text{wall},i}\right]$	(S4)

From wall cell i to heating and cooling jacket i	$\dot{Q}_{\text{wall}-\text{hc},i} = (\alpha A)_{\text{wall}-\text{hc},i}\left[T_{\text{wall},i} - T_{\text{hc},i}\right]$	(S5)

Model of the gas volume (gas)

Overall mass balance	$\dfrac{d\rho_{\text{gas},i}}{d\tau} = \dfrac{1}{V_{\text{gas},i}}\left[\dot{m}_{\text{conv},i-1} + \dot{m}_{\text{conv},i} + \displaystyle\sum_{j=1}^{n_{\text{adsorbate}}} \dot{m}_{\text{LDF},i,j}\right]$	(S6)

Balance of component j	$$\frac{dw_{j,i}}{d\tau} = \frac{1}{V_{\text{gas},i}\,\rho_{\text{gas},i}} \left[\dot{m}_{\text{conv},i-1} \begin{cases} w_{j,i-1}, & \dot{m}_{\text{conv},i-1} \geq 0 \\ w_{j,i}, & \dot{m}_{\text{conv},i-1} < 0 \end{cases} \right. \\ \left. + \dot{m}_{\text{conv},i} \begin{cases} w_{j,}, & \dot{m}_{\text{conv},i} \geq 0 \\ w_{j,i+1}, & \dot{m}_{\text{conv},i} < 0 \end{cases} + \dot{m}_{\text{LDF},j} \right. \\ \left. - w_{j,i} V_{\text{gas},i}\, \frac{d\rho_{\text{gas},i}}{d\tau} \right]$$	(S7)
Energy balance	$$\frac{dh_{\text{gas},i}}{d\tau} = \frac{1}{V_{\text{gas},i}\,\rho_{\text{gas},i}} \left[\dot{Q}_{\text{gas}-\text{sor},i} \right. \\ \left. + \dot{m}_{\text{conv},i-1} \begin{cases} h_{\text{gas},i-1}, & \dot{m}_{\text{conv},i-1} \geq 0 \\ h_{\text{gas},i}, & \dot{m}_{\text{conv},i-1} < 0 \end{cases} \right. \\ \left. + \dot{m}_{\text{conv},i} \begin{cases} h_{\text{gas},i}, & \dot{m}_{\text{conv},i} \geq 0 \\ h_{\text{gas},i+1}, & \dot{m}_{\text{conv},i} < 0 \end{cases} \right. \\ \left. + \sum_{j=1}^{n_{\text{adsorbate}}} \dot{m}_{\text{LDF},i,j} \begin{cases} h_{\text{sor},i,j}, & \dot{m}_{\text{LDF},i,j} \geq 0 \\ h_{\text{gas},i}, & \dot{m}_{\text{LDF},i,j} < 0 \end{cases} \right. \\ \left. - h_{\text{gas},i} V_{\text{gas},i}\, \frac{d\rho_{\text{gas},i}}{d\tau} + V_{\text{gas},i}\, \frac{dp_{\text{gas},i}}{d\tau} \right]$$	(S8)

Model of the adsorbent (sor):

Balance of component j	$$\frac{dX_{\text{sor},i,j}}{d\tau} = \frac{1}{m_{\text{sor},i}}\,\dot{m}_{\text{LDF},i,j}$$	(S9)
Energy balance	$$\frac{dT_{\text{sor},i}}{d\tau} = \frac{1}{m_{\text{sor},i}\left[c_{\text{sor}} + \sum_{j=1}^{n_{\text{adsorbate}}} c_{\text{adsorbate},i,j} X_{\text{sor},i,j}\right]} \\ \cdot \left[\sum_{j=1}^{n_{\text{adsorbate}}} \dot{m}_{\text{LDF},i,j} \begin{cases} h_{\text{sor},i,j}, & \dot{m}_{\text{LDF},i,j} \geq 0 \\ h_{\text{gas},i}, & \dot{m}_{\text{LDF},i,j} < 0 \end{cases} + \dot{Q}_{\text{gas}-\text{sor},i} \right. \\ \left. + \dot{Q}_{\text{sor}-\text{wall},i} \right. \\ \left. + \sum_{j=1}^{n_{\text{adsorbate}}} (h_{\text{sor},i,j} - \Delta h_{\text{ads},j})\, \frac{dX_{\text{sor},i,j}}{d\tau} \right]$$	(S10)

Model of the wall (wall)

Energy balance	$$m_{\text{wall},i} c_{\text{wall}}\, \frac{dT_{\text{wall},i}}{d\tau} = \dot{Q}_{\text{sor}-\text{wall},i} + \dot{Q}_{\text{wall}-\text{hc},i}$$	(S11)

Model of the gas volume (gas): Main equations of the gas volume model were three transient balance equations: i) Overall mass balance (eqn S6), ii) mass balance of component j (eqn S7), and iii) energy balance (eqn S8). Thus, the selected differential states of the $i^{th.}$cell were the gas density ρ_i, the mass fractions $w_{j,i}$ for each component j of the gas phase, and the temperature $T_{\mathrm{gas},i}$.

Model of the adsorbent (sor): The adsorbent cell was based on the adsorbent cell developed by Bau et al.[6] but was adapted for more than one adsorbate in this work. The adsorbent cell had transient component/mass (eqn S9) and energy balances (eqn S10) as the main equations. Selected differential states were the adsorbent temperature $T_{\mathrm{sor},i}$ and the loading of each component $X_{\mathrm{sor},j,i}$.

Model of the wall (wall): The wall cell was modelled by a transient energy balance (eqn S11) with the temperature $T_{\mathrm{wall},i}$ as the differential state.

Heat and mass transport: Heat flow rates between the gas volume and the adsorbent cell; the adsorbent cell and the wall cell; and the wall cell and the environment were modelled by a temperature difference between the components and the corresponding product of heat transfer coefficients and areas $(\alpha A)_j$. The convective mass transport from gas volume i to $i + 1$ was calculated by the total pressure gradient and the mass transfer coefficient β. The mass transport from the gas volume to the adsorbent cell was calculated by the linear driving force approach [7] with the mass transfer coefficient $k_{\mathrm{LDF},j}$ for each component j.

2.1 Details of the Dynamic DAC Column Model

Adsorption equilibrium models

Characterisation of the adsorption equilibrium is the core of the dynamic DAC column model. We examined amine-functionalised cellulose called APDES-NFC[8] as the adsorbent. To model the adsorption equilibrium, we used the heuristic model proposed by Stampi-Bombelli et al.[9], where the CO_2 adsorption is modelled by a modified Toth isotherm and the water adsorption by the Guggenheim–Anderson de Boer isotherm (GAB). In particular, the modified Toth isotherm was extended by interaction parameters. These interaction parameters enhance CO_2 adsorption if water is co-adsorbed. Note that it is crucial to represent the co-adsorption sufficiently for the accuracy of the process model.[1] For the adsorbent Lewatits® VP OC 1065, two models were presented by Young et al.:[1] A mechanistic and a weighted-average dual-site Toth model. Both models outperformed the heuristic model from Stampi-Bombelli et al.[1] However, for the adsorbent APDES-NFC studied in this paper, the co-adsorption between CO_2 and water is well described by the heuristic model (Fig. 3), which is why we applied it. Tab. 2 shows all equations applied to characterise the co-adsorption of CO_2 and H_2O on APDES-NFC, and parameters for the equations eqn S12-S17 are summarised in Tab. 3.

Tab. 2   Modified Toth equation (eqn S12) to describe CO_2 adsorption on amine-functionalised cellulose (APDES-NFC) under dry and humid conditions, and the Guggenheim–Anderson de Boer

equation to describe H₂O adsorption. Eqn S13 to S15 indicate temperature dependencies of the parameters used in the Toth equation. The heuristic co-adsorption model is based on Stampi-Bombelli et al..[9]

Co-adsorption equilibrium model for CO_2

Modified Toth equation[9]

$$X_{\text{sor,CO}_2}(T, p_{\text{CO}_2}, X_{\text{sor,H}_2\text{O}})$$
$$= \frac{X_{\text{sor,CO}_2}^{\infty,\text{mod}}(T, X_{\text{sor,H}_2\text{O}})\, b^{\text{mod}}(T, X_{\text{sor,H}_2\text{O}})\, p_{\text{CO}_2}}{\left[1 + \left(b^{\text{mod}}(T, X_{\text{sor,H}_2\text{O}})p_{\text{CO}_2}\right)^{t(T)}\right]^{\frac{1}{t(T)}}}$$

(S12)

---

with:

$$X_{\text{sor,CO}_2}^{\infty,\text{mod}}(T, X_{\text{sor,H}_2\text{O}})$$
$$= X_{\text{sor,CO}_2}^{\infty,0} \exp\left(\chi\left(1 - \frac{T}{T_0}\right)\right)\left[\frac{1}{1 - \gamma X_{\text{sor,H}_2\text{O}}}\right] \quad \text{for } \gamma > 0$$

(S13)

$$b^{\text{mod}}(T, X_{\text{sor,H}_2\text{O}})$$
$$= b^0 \exp\left(\frac{\Delta H^0}{RT_0}\left(\frac{T_0}{T} - 1\right)\right)\left[1 + \kappa X_{\text{sor,H}_2\text{O}}\right]$$
$$\text{for } \kappa > 0$$

(S14)

$$t(T) = t^0 + \alpha\left(1 - \frac{T_0}{T}\right)$$

(S15)

Adsorption equilibrium model for H_2O

Guggenheim–Anderson de Boer[9]

$$X_{\text{sor,H}_2\text{O}}(T, p_{\text{H}_2\text{O}})$$
$$= c_{\text{m}} \frac{c_G K_{\text{ads}} \frac{p_{\text{H}_2\text{O}}}{p_{\text{H}_2\text{O}}^{\text{sat}}(T)}}{\left(1 - K_{\text{ads}} \frac{p_{\text{H}_2\text{O}}}{p_{\text{H}_2\text{O}}^{\text{sat}}(T)}\right)\left(1 + (c_G - 1)K_{\text{ads}} \frac{p_{\text{H}_2\text{O}}}{p_{\text{H}_2\text{O}}^{\text{sat}}(T)}\right)}$$

(S16)

---

with:[10]

$$p_{\text{H}_2\text{O}}^{\text{sat}}(T)$$

(S17)

Tab. 3 Parameters of the co-adsorption model used to describe the adsorption of CO_2 and H_2O on the adsorbent APDES-NFC adapted from literature.[9]

Parameters of the modified Toth isotherm

$X_{sor,CO_2}^{\infty,0}$ in $\frac{mol}{kg}$	χ in $-$	T_0 in K	γ in $-$	b^0 in $\frac{1}{Pa}$	ΔH^0 in $\frac{J}{mol}$	κ in $-$	t^0 in $-$	α in $-$
2.38	0	296	0.0061	0.07074	-57047	28.907	0.4148	-1.606

Parameters of the Guggenhein–Anderson de Boer isotherm

c_m in $\frac{mol}{kg}$	c_G in $-$	K_{ads} in $-$
36.48	0.1489	0.5751

Fig. 3 shows the comparison of the co-adsorption model with literature data for CO_2 adsorption and H_2O adsorption.
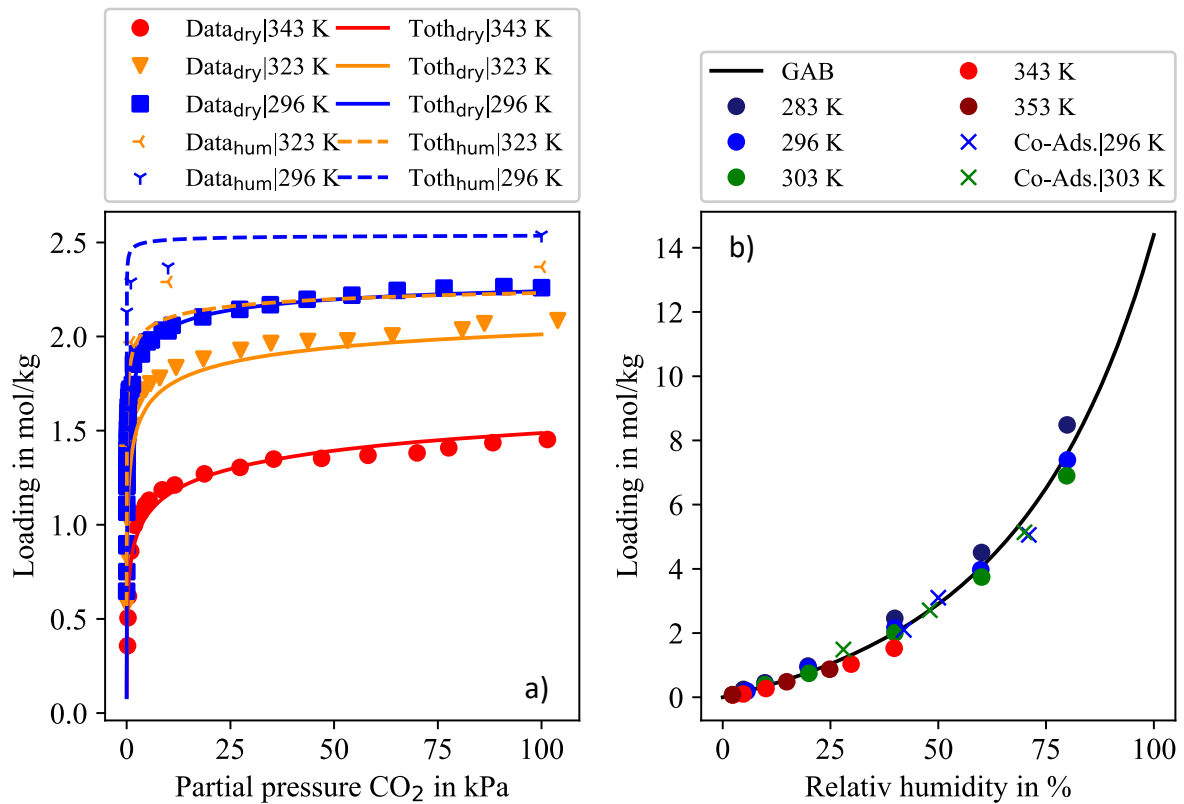
Fig. 3 Fitted equilibrium adsorption model for a) CO_2 (eqn S11, Toth isotherm) and b) H_2O (eqn S15, GAB isotherm) on amine-functionalised cellulose (APDES-NFC) based on Stampi-Bombelli

et al.[9]. **Solid lines mark pure adsorption (dry) and dashed lines co-adsorption (humid conditions (hum) with $p_{H_2O} = 2.55$ kPa). Symbols are experimental data from Gebald et al.[8]**

DAC adsorption column model parameterisation

We parameterised the DAC adsorption column model based on data from Stampi-Bombelli et al.[9] All relevant model parameters are listed in Tab. 4.

Tab. 4   Parameters of the DAC adsorption column model according to Stampi-Bombelli et al.[9]

Column geometries			
Column length:	L_{col}	0.01	m
Inner column diameter:	D_{in}	0.08	m
Outer column diameter:	D_{out}	0.082	m
Void fraction $\left(1 - \frac{\rho_{bed}}{\rho_{material}}\right)$:	ε	0.9652	-
Specific heat capacity of the wall:	c_{wall}	4e6	J/K/m^3
Kinetic parameters			
Heat transfer coefficient, gas to adsorbent:	$(\alpha A)_{gas-sor,i}$	1e4	W/K
Heat transfer coefficient, adsorbent to wall:	$(\alpha A)_{sor-wall,i}$	3	W/m^2/K
Heat transfer coefficient, wall to heating/cooling jacket:	$(\alpha A)_{wall-hc,i}$	26	W/m^2/K
CO_2 mass transfer coefficient (LDF):	k_{LDF,CO_2}	2e-4	1/s
H_2O mass transfer coefficient (LDF):	k_{LDF,H_2O}	2e-3	1/s
Adsorbent			
Specific heat capacity of the adsorbent:	c_{sor}	2.07e3	J/K/kg
Heat of adsorption of CO_2:	$\Delta h_{ads,CO_2}$	-57e3	J/mol
Heat of adsorption of H_2O:	$\Delta h_{ads,H_2O}$	-49e3	J/mol
Particle diameter	d_{par}	7.5e-3	m

Pressure drop correlations

A typical pressure drop equation for packed beds is the Ergun equation. The Ergun equation assumes a parallel circuit of flow channels can represent the flow through a packed bed.[11] A particular form of the Ergun equation is the Kozeny–Carman equation. In the Kozeny–Carman

equation, a term of the pressure loss coefficient is neglected. The neglected term is mainly responsible for the turbulent region of the flow. Therefore, the Kozeny–Carman equation is more suitable for low flow velocities.[11] As the DAE solver used (CVoder) solves the Kozeny–Carman equation much more efficiently than the Ergun equation and only low flow velocities were investigated, we used the Kozeny–Carman equation for all pressure loss calculations. However, to get even closer to the Ergun equation's pressure loss results, we added the parameter $\zeta_{\mathrm{mod,kc}}$ to the Kozeny–Carman equation and fitted this parameter to match pressure loss calculated by the Ergun equation in the reference case (Fig. 4).

Both the Ergun equation and the Kozeny–Carman equation are directly dependent on the fluid properties in the respective gas cell (via density $\rho_{\mathrm{gas},i}$ and dynamic viscosity $\eta_{\mathrm{gas},i}$): The pressure drop influences the fluid properties (fluid properties: $f(p,T)$) and vice versa. Thus, the DAE solver cannot unambiguously resolve this relationship, meaning the solution must be determined iteratively. An iterative solving of the equation system always increases computational effort. To further reduce computational effort, pressure drops were always calculated with the fluid properties at the adsorption column inlet. Since the inlet fluid properties do not depend on the pressure drop, it is possible to avoid iteration when solving the equation system. This assumption is reasonable as the fluid properties change only slightly over the adsorption column length. Thus, the effect of the assumption on the pressure drop is minimal.

Tab. 5 includes the Ergun equation, the Kozeny–Carman equation, and their auxiliary equations.

Tab. 5 Equations for the pressure drop models Ergun and Kozeny–Carman.

Pressure drop models		
Ergun equation[7,11]	$\Delta p_{i \to i+1} = \zeta_{\mathrm{ergun}} L_i \; \dfrac{\rho_{\mathrm{gas},i}}{2} \dfrac{1}{d_{\mathrm{H}}} \left(\dfrac{v_{\mathrm{conv},i}}{\varepsilon} \right)^2$	(S18)
with:	$d_{\mathrm{H}} = \dfrac{2}{3} \dfrac{\varepsilon}{1-\varepsilon} \; d_{\mathrm{par}}$	(S19)
	$v_{\mathrm{conv},i} = \dfrac{\dot{m}_{\mathrm{conv},i}}{\frac{\pi}{4} D_{\mathrm{in}}^2 \varepsilon \rho_{\mathrm{gas},i}}$	(S20)
	$\zeta_{\mathrm{ergun}} = \dfrac{133.\overline{3}}{\mathrm{Re}} + 2.\overline{3}$	(S21)
	$\mathrm{Re} = \dfrac{\rho_{\mathrm{gas},i} v_{\mathrm{conv},i} d_H}{\eta_{\mathrm{gas},i} \varepsilon}$	(S22)
Kozeny–Carman equation [11]	$\Delta p_{i \to i+1} = \zeta_{\mathrm{mod,kc}} \, L_i \; \dfrac{\rho_{\mathrm{gas},i}}{2} \dfrac{1}{d_{\mathrm{H}}} \left(\dfrac{v_{\mathrm{conv},i}}{\varepsilon} \right)^2$	(S23)
with:	$\zeta_{\mathrm{mod,kc}} = 1.552 \dfrac{144}{\mathrm{Re}}$	(S24)

Fig. 4 shows the Kozeny–Carman equation to approximate the Ergun equation well. The equations particularly agree well at lower mass flow rates and, thus, lower flow velocities. The vertical line shows the reference mass flow rate: Ergun equation and Kozeny-Carman equation result in the same pressure drop at this mass flow rate.
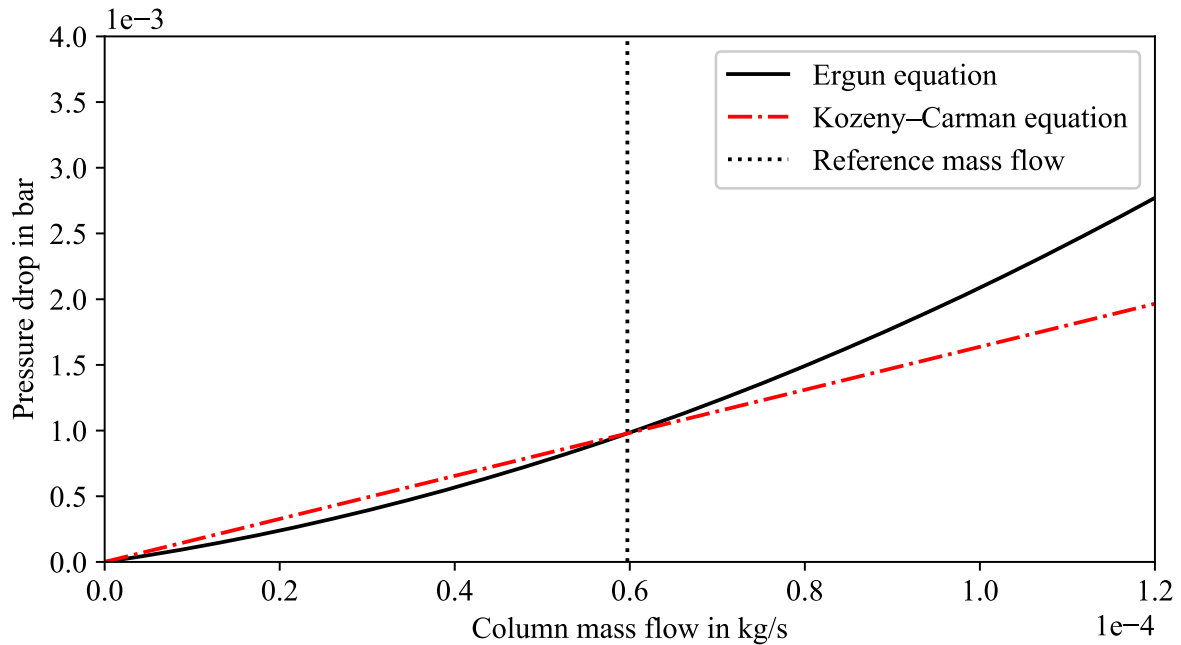
Fig. 4 **Pressure drop over the adsorption column parameterised as specified in Tab. 4. The pressure drop is calculated at 20 °C and absolute pressure of 1 bar for dry air over the mass flow rate. The figure shows the pressure drop calculated with i) the Ergun equation (solid black line) and ii) the Kozeny–Carman equation (dashed-dotted line).**

Literature base case

We used literature data of an identically parameterised model to validate our model. Tab. 6 gives the process design used for comparing the two models.

Tab. 6 Process design and ambient based on the base case of Stampi-Bombelli et al.[9]

Ambient conditions		
Dry air composition χ_{N_2}; χ_{O_2}; χ_{CO_2}	0.790133; 0.20946; 407e-6	mol/mol
Ambient temperature T_{amb}	20	°C
Ambient pressure p_{amb}	1	bar
Relative humidity φ_{amb}	49.166	%
I) Adsorption phase		
Mass flow rate $\dot{m}_{ads}$	5.8935e-5	kg/s

Phase duration τ_{ads}	13772	s

II) Blowdown phase

Blowdown pressure p_{des}	0.05	bar
Phase duration τ_{blow}	30	s

III) Heating phase

Heating temperature T_{des}	95	°C
Phase duration τ_{heat}	704	s

IV) Desorption phase

Steam mass flow rate $\dot{m}_{ste}$	7.35673e-7	kg/s
Phase duration τ_{des}	30000	s

Fig. 5 shows the time courses of CO_2 loading (a), H_2O loading (b), and different temperatures (c) for both our model (lines) and the literature model (marker). It becomes evident that all time courses conform with the literature model.
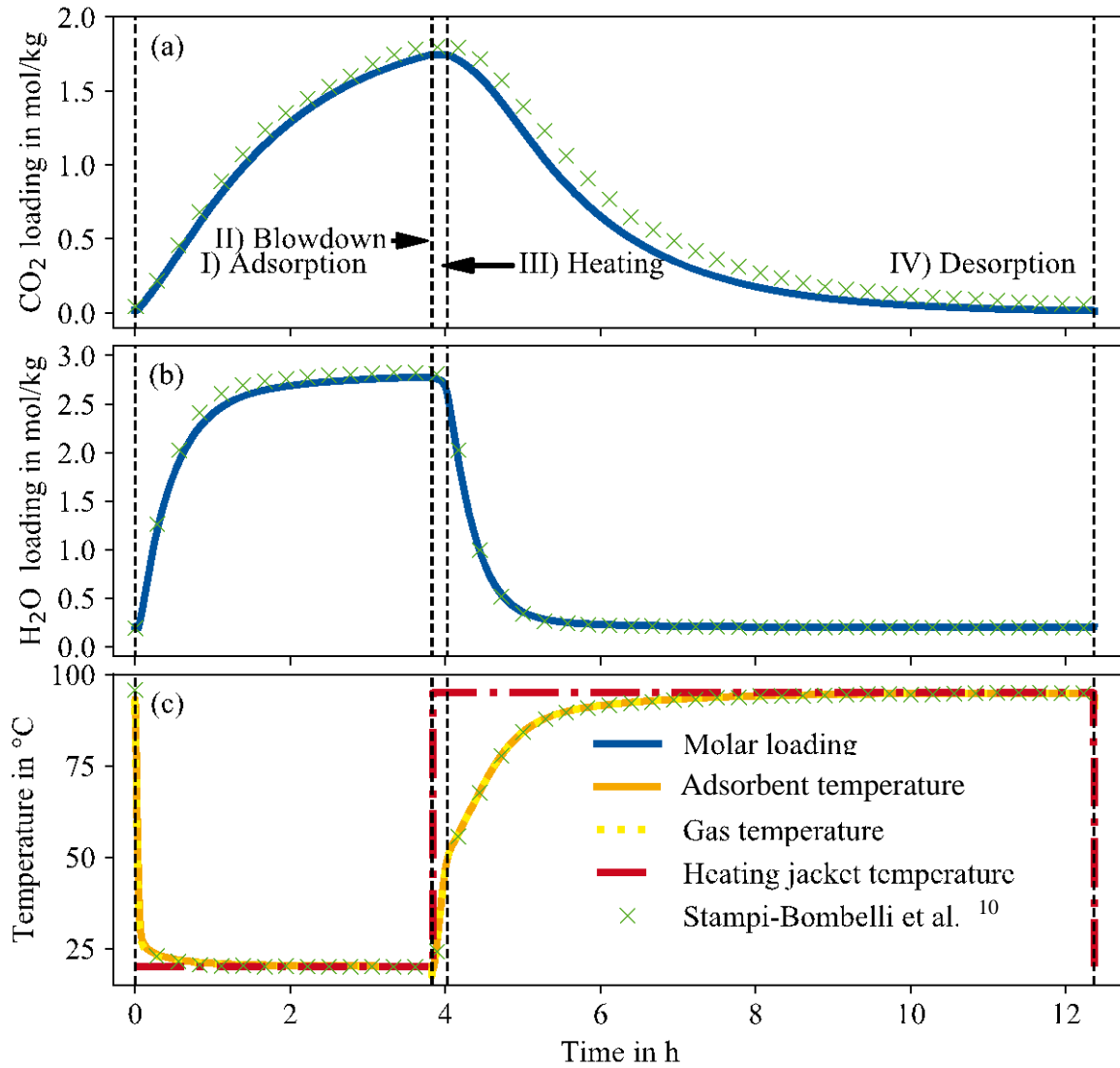
Fig. 5 Time courses of selected differential states of the last adsorption column cell at a cyclic steady-state condition for a base case of a S-TVSA cycle (Tab. 6). The vertical dashed lines mark the beginning and end of the four phases of the cycle. Phase II) (Blowdown) is so short that it is not visible in the plot.

2.2 Details of the Dynamic DAC Plant Model

Table 7 shows i) the exergetic efficiency of the <u>H</u>igh <u>T</u>emperature <u>H</u>eat <u>P</u>ump (HTHP), ii) the efficiency of the fan, and iii) the efficiency of the vacuum pump depending on the pressure.

Table 7: Efficiencies for the high-temperature heat pump (hthp), the fan (fan), and the vacuum pump (vac).

Symbol	Efficiency	Reference
$\eta_{ex,hthp}$	60 %	[12]
η_{fan}	50 %	[9]
η_{vac}	30 % ($p_{des} \leq 0.01$ bar) 30-70 % ($p_{des} = 0.01 - 0.1$ bar) 70 % ($p_{des} \geq 0.1$ bar)	[9]

2.3 Details of the Key Performance Indicators

For calculating the <u>K</u>ey <u>P</u>erformance <u>I</u>ndicators (KPIs), we used the following definitions for the total mechanical and thermal energy of the DACCS system. As the DAC plant had the only heat requirement of the DACCS system, the total thermal energy requirement Q_{total} was the same as for the DAC plant $Q_{\text{DAC,total}}$,

$$Q_{\text{total}} = Q_{\text{DAC,total.}} \tag{S24}$$

The total thermal energy for the DAC plant,

$$Q_{\text{DAC,total}} = \int_{\tau_2}^{\tau_3} \dot{Q}_{\text{heat}}\, t + \int_{\tau_3}^{\tau_4} \dot{Q}_{\text{des}}\, dt, \tag{S25}$$

was defined as the sum of the integrated heat flow rates of the heating phase $\dot{Q}_{\text{heat}}$ and of the desorption phase $\dot{Q}_{\text{des}}$. Integral limits were $\tau_2 = \tau_{\text{ads}} + \tau_{\text{blow}}$, $\tau_3 = \tau_{\text{ads}} + \tau_{\text{blow}} + \tau_{\text{heat}}$, and $\tau_4 = \tau_{\text{ads}} + \tau_{\text{blow}} + \tau_{\text{heat}} + \tau_{\text{des}}$.

As only the DAC plant needed to be cooled, the total dissipated heat was equal to the dissipated heat of the DAC plant:

$$Q_{\text{recool}} = Q_{\text{DAC,recool.}} \tag{S26}$$

The dissipated heat of the DAC plant $Q_{\text{DAC,recool}}$,

$$Q_{\text{DAC,recool}} = \int_{\tau_3}^{\tau_4} \dot{Q}_{\text{cond}}\, t + \int_{\tau_4}^{\tau_5} \dot{Q}_{\text{cool}}\, t, \tag{S27}$$

composed of the integrated heat flow rate for cooling and condensing the water in the product stream $\dot{Q}_{\text{cond}}$ and the integrated heat flow rate during the cooling phase $\dot{Q}_{\text{cool}}$, with integral limit $\tau_5 = \tau_{\text{ads}} + \tau_{\text{blow}} + \tau_{\text{heat}} + \tau_{\text{des}} + \tau_{\text{cool}}$.

In contrast to thermal energy, other components of the DACCS system also demanded mechanical energy in addition to the DAC plant. The total mechanical energy W_{total} was calculated as the sum of the mechanical demands of all subsystems:

$$W_{\text{total}} = W_{\text{DAC}} + W_{\text{comp}} + W_{\text{rec}} + W_{\text{inj}}. \tag{S28}$$

The mechanical energy demand for the DAC plant W_{DAC},

$$W_{\text{DAC}} = \int_0^{\tau_1} \dot{W}_{\text{fan}}\, dt + \int_{\tau_1}^{\tau_2} \dot{W}_{\text{vac,blow}}\, dt + \int_{\tau_2}^{\tau_3} \dot{W}_{\text{vac,heat}}\, dt + \int_{\tau_3}^{\tau_4} \dot{W}_{\text{vac,des}}\, dt$$
$$+ W_{\text{recool}} + W_{\text{HTHP}}, \tag{S29}$$

was calculated as the sum of the integrated powers of the fan $\dot{W}_{\text{fan}}$, the vacuum pumps $\dot{W}_{\text{vac}}$, and the energy demand for the recooling W_{recool}, with integral limit $\tau_1 = \tau_{\text{ads}}$. The vacuum pump was active in three phases: Blowdown (blow), heating (heat), and desorption (des). The mechanical energies for the four system components i) compressor W_{comp}, ii) transportation W_{rec}, iii) injection W_{inj}, and iv) recooling W_{recool} were calculated with eqn 12 and eqn 11 (main text), respectively.

Besides the total mechanical and thermal energy, the mass of the product m_{prod} is a crucial metric for evaluating the DACCS system. The product m_{prod},

$$m_{\text{prod}} = \int_{\tau_3}^{\tau_4} (\dot{m}_{\text{des}} - \dot{m}_{\text{cond}})\, dt, \tag{S30}$$

is the integrated difference between the desorbed mass flow rate $\dot{m}_{\text{des}}$ and the condensed water mass flow rate $\dot{m}_{\text{cond}}$. The total mass of captured CO_2 $m_{\text{co}_2\text{,cap}}$,

$$m_{\text{co}_2\text{,cap}} = \int_{\tau_3}^{\tau_4} \dot{m}_{\text{des}}\, w_{\text{co}_2}\, dt, \tag{S31}$$

was defined as the integrated mass flow rate during the desorption phase $\dot{m}_{\text{des}}$ multiplied by the mass fraction of CO_2 (w_{co_2}). The stored mass of CO_2 ($m_{\text{co}_2\text{,sto}}$) is defined as the mass of captured CO_2 minus potential leakages during transport and storrage CC_{leak} as:

$$m_{\text{co}_2\text{,sto}} = m_{\text{co}_2\text{,cap}} - CC_{\text{leak}} \tag{S32}$$

However, as we assume for the entire paper that there are no leakages, no distinction between $m_{\text{co}_2\text{,sto}}$ and $m_{\text{co}_2\text{,cap}}$ is made in the main text. Besides the mass of stored CO_2, GHG emissions are needed during the removal process to calculate the $\underline{C}$arbon $\underline{R}$emoval $\underline{E}$fficiency (CRE) (eqn 4 (main text)). The GHG emissions can be further divided into emissions due to the energy supply (CC_{ene}), the construction and end-of-life of the DACCS system (CC_{cons}) and the adsorbent consumption (CC_{sor}). The emissions due to the energy supply are defined by the total energy demand W_{total} and the electricity's GHG emissions (cf_{el}) as:

$$CC_{\text{ene}} = cf_{\text{el}}\, W_{\text{total}}. \tag{S33}$$

The emissions for construction and end-of-life of the DACCS system (CC_{cons}) adds up the emissions from the construction and end of life of the DAC plant ($cc_{\text{cons,DAC}}$) and all other components such as pipelines, etc $cc_{\text{cons,CS}}$.as:

$$CC_{\text{cons}} = cc_{\text{cons,DAC}}\, m_{\text{co}_2\text{,cap}} + cc_{\text{cons,CS}}\, m_{\text{co}_2\text{,cap}}. \tag{S34}$$

However all other emissions except those from the construction and end of life of the DAC plant are neglected in this paper. Finally, the emissions due to adsorbent consumption are calculated as follows:

$$CC_{\text{sor}} = cc_{\text{sor}} m_{\text{co}_2\text{,cap}}. \tag{S35}$$

2.4 Details of the case study and optimisation framework

The degrees of freedom of the process design optimisation were the following: Mass flow rate $\dot{m}_{\text{ads}}$ of air during the adsorption phase; phase times τ_{ads}, τ_{blow}, τ_{heat}, and τ_{des}; and desorption conditions p_{des}, T_{des}, and $\dot{m}_{\text{ste}}$. The upper and lower bounds of the process design variables are presented in Tab. 8.

Tab. 8 Process design variables with lower and upper bounds used for process optimisation.

Process design variable	Lower bound	Upper bound

$\dot{m}_{ads}$	1e-5	2e-4	$\dfrac{kg}{s}$
τ_{ads}	3000	40000	s
τ_{blow}	30	30	s
τ_{heat}	50	2000	s
τ_{des}	5000	40000	s
p_{des}	0.01	0.3	bar
T_{des}	80	s100	°C
$\dot{m}_{ste}$	1e-9	1e-7	$\dfrac{kg}{s}$

The ambient conditions, such as temperature and relative humidity, have a crucial influence on the performance of DACCS systems.[13] However, a variation of the ambient conditions was beyond the scope of this work. Therefore, we exemplarily used the annual average values for the city of Aachen in Germany for all calculations. The yearly average values from the years 1991-2021 are summarised in Tab. 9.

Tab. 9   Ambient conditions used for all simulations.

Ambient conditions			Source
Ambient temperature T_{amb}	10.133	°C	[14]
Relative humidity φ_{amb}	77	%	[14]
Ambient pressure p_{amb}	1.01325	bar	-
Mole fraction of CO_2 in dry air χ_{CO_2}	407	ppm	-

3. Results

3.1 Details of the Plant Productivity and Reference Cases
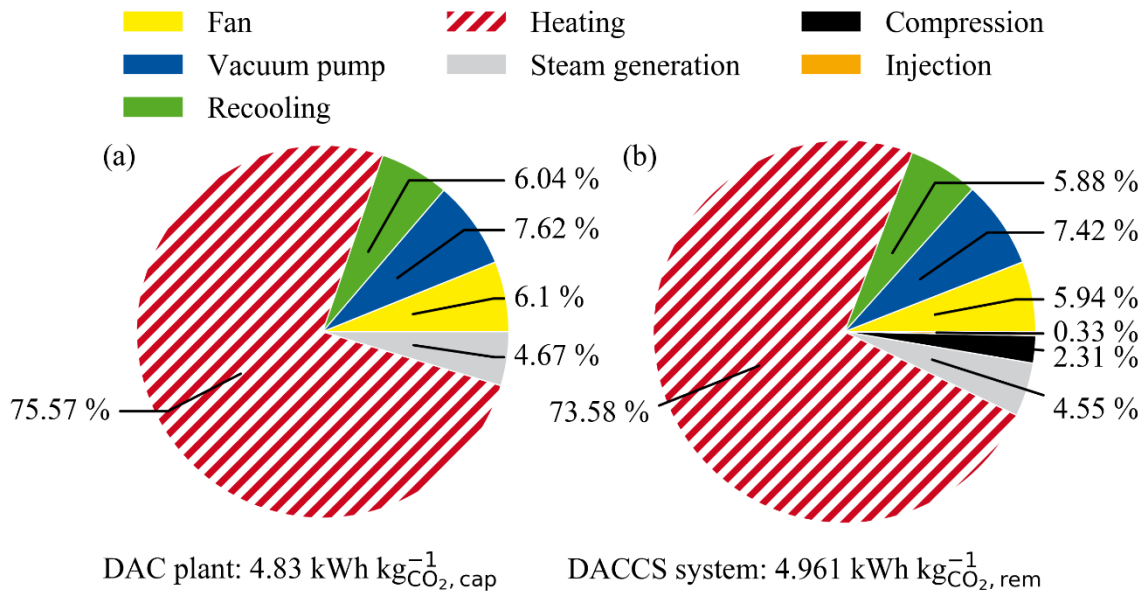
Tab. 10. Summarises the process design variables for the reference cases of a TVSA and a S-TVSA-

Tab. 10 List of the process design variables for the reference case of the TVSA and the S-TVSA cycle.

Process design variables	Reference case: S-TVSA	
$\dot{m}_{ads}$	9.30274027e-05	$\dfrac{kg}{s}$
τ_{ads}	1.03463744e+04	s
τ_{blow}	30	s

τ_{heat}	6.45587617e+01	s
τ_{des}	1.30435829e+04	s
p_{des}	1.00000e-02	bar
T_{des}	99.303946	°C
$\dot{m}_{ste}$ (for S-TVSA)	7.35673e-8	$\dfrac{kg}{s}$

In addition to the specific energy demands for the reference case of the TVSA cycle in the main text, Fig. 6 shows the specific energy demands for the reference case of the S-TVSA for a DAC plant and a DACCS system. In contrast to the TVSA, the S-TVSA required slightly more energy per mass of captured CO_2. However, as the steam purge accelerates the desorption, the reference case of the S-TVSA achieved a Plant Productivity (PP) of 4.12 kt_{CO_2} yr^{-1} instead of 4 kt_{CO_2} yr^{-1}.

Legend: Fan (yellow), Heating (red hatched), Compression (black), Vacuum pump (blue), Steam generation (grey), Injection (orange), Recooling (green)

(a)
6.04 %
7.62 %
6.1 %
4.67 %
75.57 %

(b)
5.88 %
7.42 %
5.94 %
0.33 %
2.31 %
4.55 %
73.58 %

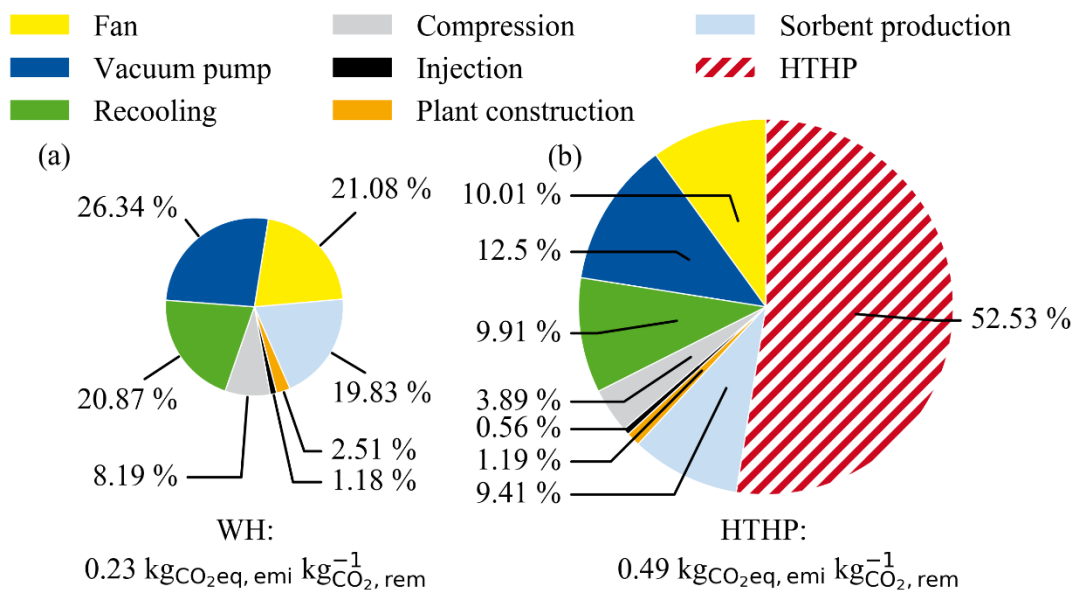DAC plant: 4.83 kWh $kg^{-1}_{CO_2, cap}$ DACCS system: 4.961 kWh $kg^{-1}_{CO_2, rem}$

Fig. 6   Specific energy demands of (a) a DAC plant based on a S-TVSA cycle and (b) a DACCS system based on a S-TVSA cycle for the reference process design. The plant productivity is 4.12 kt_{CO_2} yr^{-1}. The specific energy demand is divided into the demands heat (red), power for the fan (yellow), power for the vacuum pump (blue), and power for recooling (green). For the DACCS system, the power demands for compression and injection into the storage site are added in grey and black, respectively.

Fig. 7 shows the GHG emissions for the reference process design of the S-TVSA cycle. The specific emissions are shown for the Waste Heat (WH) case and the High-Temperature Heat Pump (HTHP) case.

Fig. 7   GHG emissions during the removal process for a DACCS system based on a S-TVSA cycle. Specific emissions are given for the reference process design with plant productivity of 4.12 kt_{CO_2} yr^{-1}: (a) WH case and (b) HTHP case. The carbon footprint of electricity is 0.166 $kg_{CO_2\text{-eq.}}$ kWh^{-1}.

3.2   Details of the impact of the KPI used for the optimisation

For Pareto frontiers of the CRE-optimal process designs of the TVSA cycle, the process design variables (τ_{ads}, τ_{heat}, τ_{des}, $\dot{m}_{ads}$, T_{des}, p_{des}) are shown in Fig. 8 for the WH case

Legend: Fan (yellow), Compression (grey), Sorbent production (light blue), Vacuum pump (blue), Injection (black), HTHP (red hatched), Recooling (green), Plant construction (orange)

(a)
26.34 %
21.08 %
20.87 %
19.83 %
8.19 %
2.51 %
1.18 %

(b)
10.01 %
12.5 %
9.91 %
3.89 %
0.56 %
1.19 %
9.41 %
52.53 %

WH:
0.23 $kg_{CO_2eq, emi}$ $kg^{-1}_{CO_2, rem}$

HTHP:
0.49 $kg_{CO_2eq, emi}$ $kg^{-1}_{CO_2, rem}$

20

and in Fig. 9 for the HTHP case. Fig. 10 shows the process design variables for the S-TVSA cycle for the WH case and Fig 11 for the HTHP case.
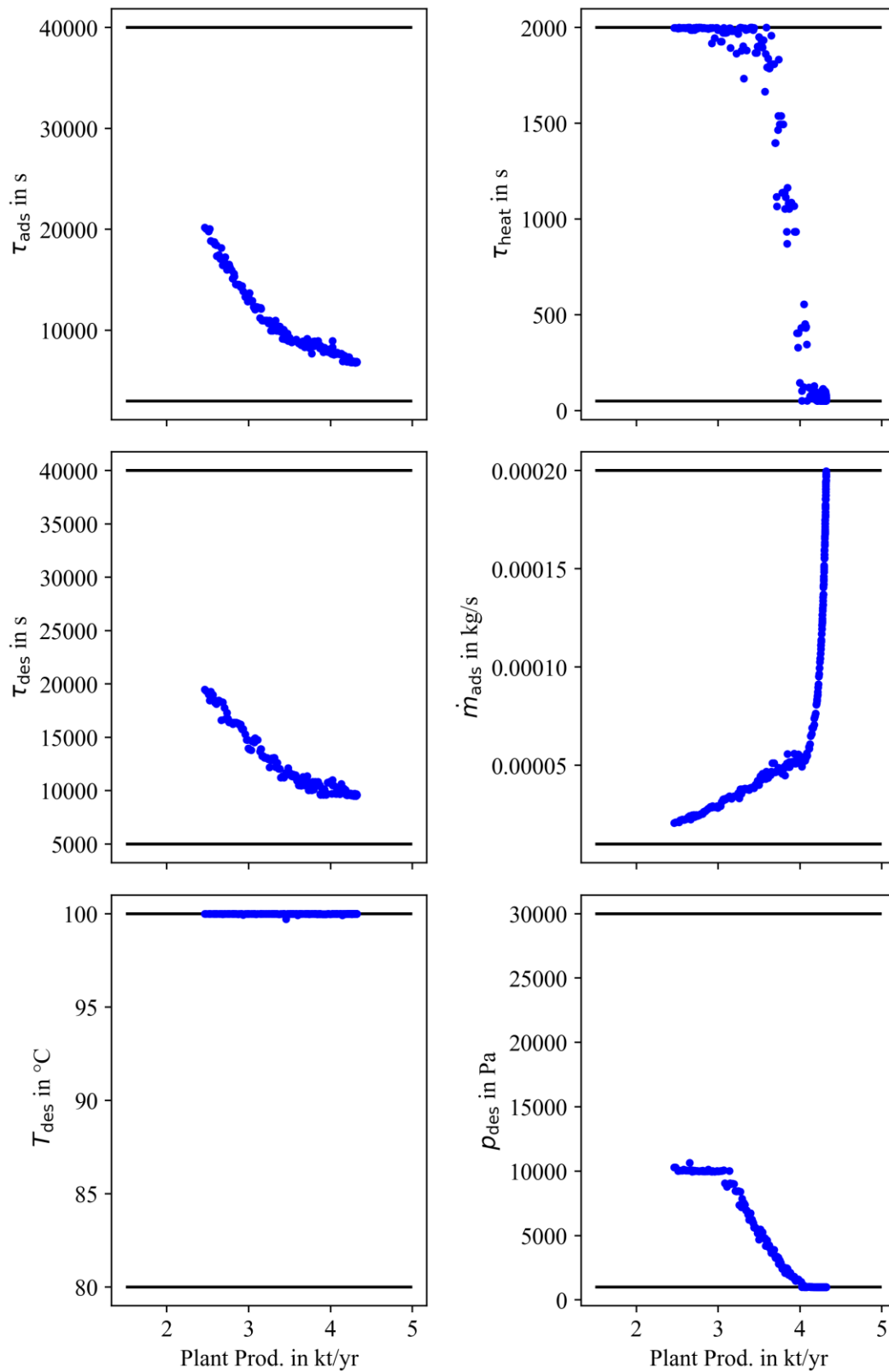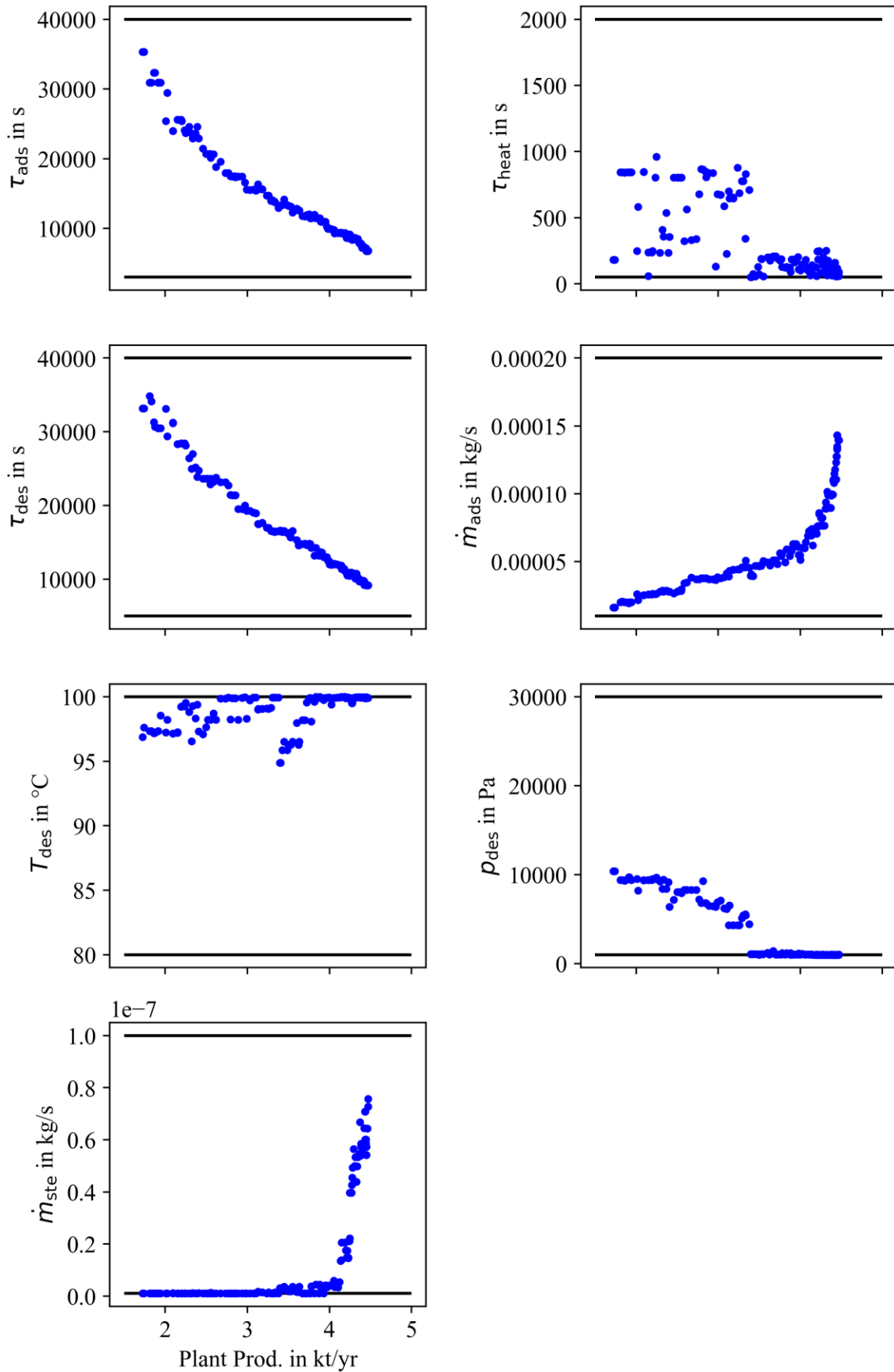

Fig. 8 Process design variables (τ_{ads}, τ_{heat}, τ_{des}, $\dot{m}_{ads}$, T_{des}, p_{des}) of the CRE-optimal Pareto frontier plotted against plant productivity for the TVSA cycle and the WH case.

21
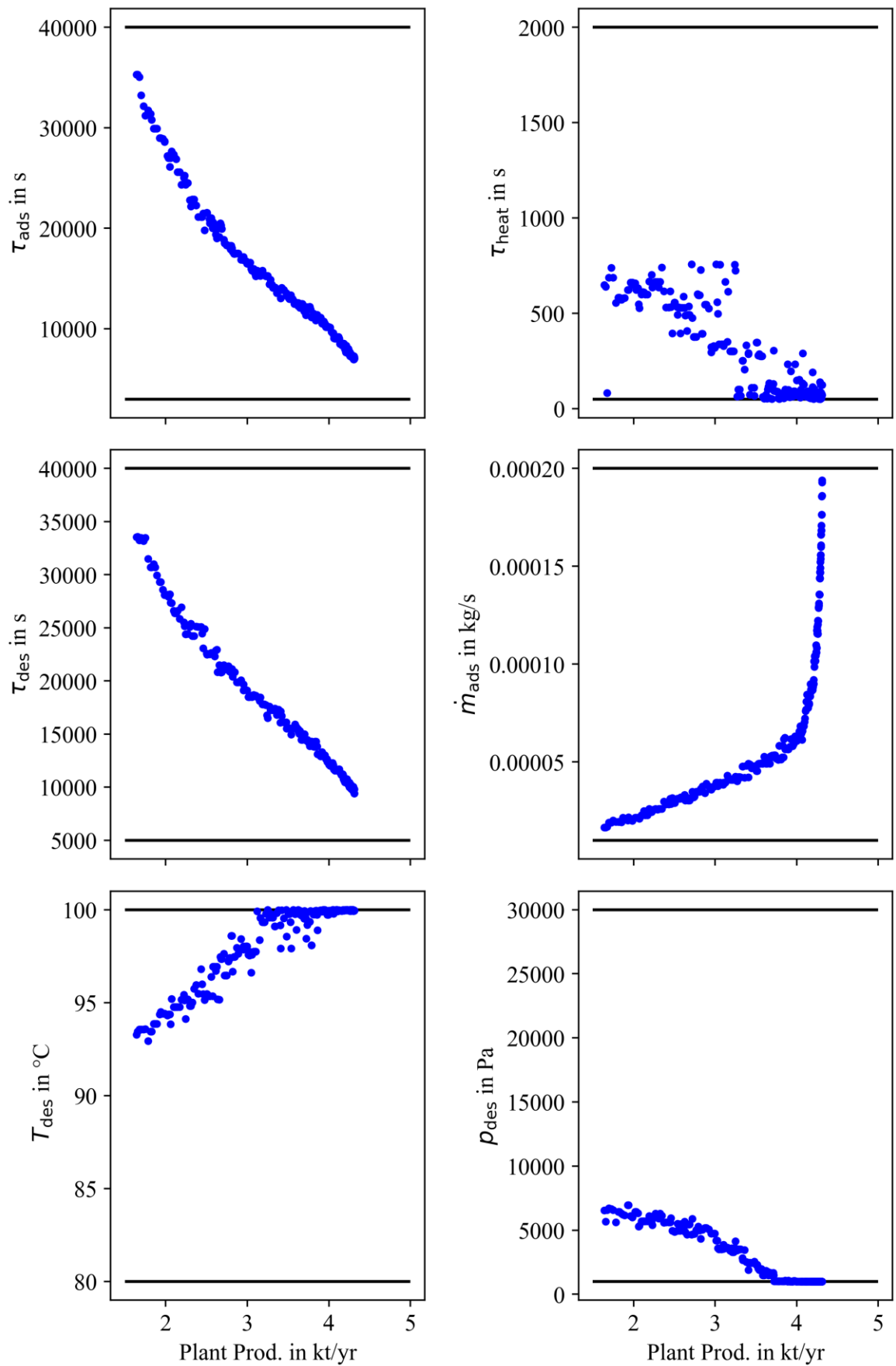
Fig. 9 Process design variables (τ_{ads}, τ_{heat}, τ_{des}, $\dot{m}_{\text{ads}}$, T_{des}, p_{des}) of the CRE-optimal Pareto frontier plotted against plant productivity for the TVSA cycle and the HTHP case.
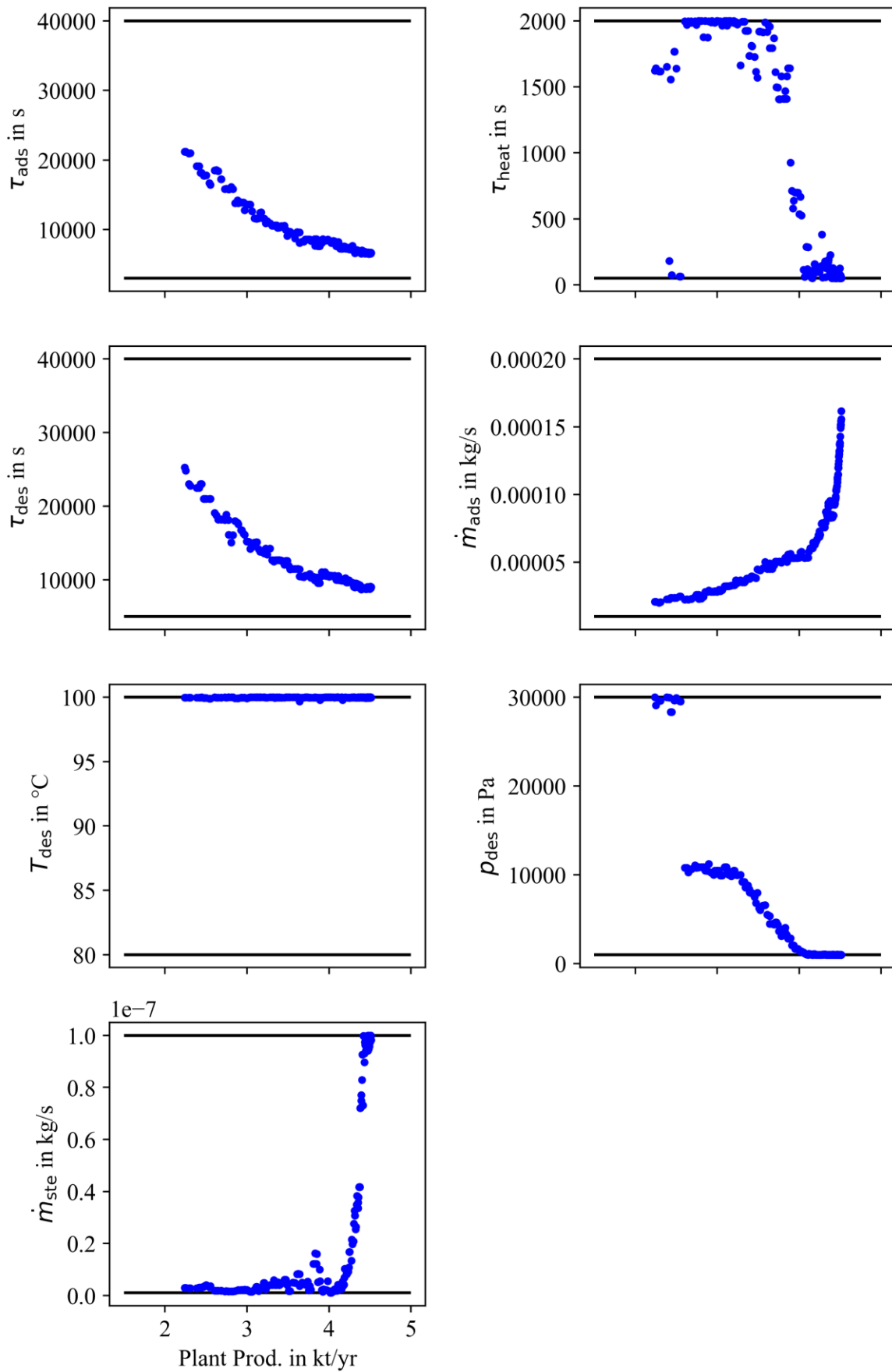
Fig. 10 Process design variables (τ_{ads}, τ_{heat}, τ_{des}, $\dot{m}_{ads}$, T_{des}, p_{des}, $\dot{m}_{ste}$) of the CRE-optimal Pareto frontier plotted against plant productivity for the S-TVSA cycle and the WH case.

Fig 11 Process design variables (τ_{ads}, τ_{heat}, τ_{des}, $\dot{m}_{ads}$, T_{des}, p_{des}, $\dot{m}_{ste}$) of the CRE-optimal Pareto frontier plotted against plant productivity for the S-TVSA cycle and the HTHP case.

References

1   J. Young, E. García-Díez, S. Garcia and M. van der Spek, *Energy Environ. Sci.*, 2021, **14**, 5377–5394.

2   M. Jahandar Lashaki, S. Khiavi and A. Sayari, *Chemical Society reviews*, 2019, **48**, 3320–3405.

3   Y. Fan and X. Jia, *Energy Fuels*, 2022, **36**, 1252–1270.

4   F. H. Harlow and J. E. Welch, *Phys. Fluids*, 1965, **8**, 2182.

5   *Modelica.UsersGuide,* available at: https://doc.modelica.org/Modelica%204.0.0/Resources/helpDymola/Modelica_UsersGuide.html, accessed 18 February 2022.

6   U. Bau, F. Lanzerath, M. Gräber, S. Graf, H. Schreiber, N. Thielen and A. Bardow, in *Proceedings of the 10th International Modelica Conference, March 10-12, 2014, Lund, Sweden*, Linköping University Electronic Press, 2014, pp. 875–883.

7   D. Bathen and M. Breitbach, *Adsorptionstechnik*, Springer Berlin Heidelberg, Berlin, Heidelberg, s.l., 2001.

8   C. Gebald, J. A. Wurzbacher, A. Borgschulte, T. Zimmermann and A. Steinfeld, *Environ. Sci. Technol.*, 2014, **48**, 2497–2504.

9   V. Stampi-Bombelli, M. van der Spek and M. Mazzotti, *Adsorption*, 2020, 1183–1197.

10 W. Wagner and A. Pruß, *Journal of Physical and Chemical Reference Data*, 2002, **31**, 387–535.

11 *VDI Heat Atlas*, Springer Berlin Heidelberg, Berlin, Heidelberg, 2010.

12 S. Deutz and A. Bardow, *Nat Energy*, 2021, **6**, 203–213.

13 J. F. Wiegner, A. Grimm, L. Weimann and M. Gazzani, *Ind. Eng. Chem. Res.*, 2022, **176**, 93.

14 *Klima Aachen: Wetter, Klimatabelle & Klimadiagramm für Aachen,* available at: https://de.climate-data.org/europa/deutschland/nordrhein-westfalen/aachen-2115/#climate-table, accessed 14 September 2022.